Nanoscale cues regulate the structure and function of macroscopic cardiac tissue constructs

Deok-Ho Kim[a,b,1], Elizabeth A. Lipke[a,1], Pilnam Kim[c], Raymond Cheong[a,b], Susan Thompson[a], Michael Delannoy[d], Kahp-Yang Suh[c,2], Leslie Tung[a,2], and Andre Levchenko[a,b,2]

[a]Department of Biomedical Engineering and [b]Institute for Cell Engineering, Johns Hopkins University, Baltimore, MD 21218; [c]School of Mechanical and Aerospace Engineering and the Institute of Bioengineering, Seoul National University, Seoul 151-742, Korea; and [d]Department of Cell Biology, Johns Hopkins University, Baltimore, MD 21205

Edited by Robert Langer, Massachusetts Institute of Technology, Cambridge, MA, and approved November 4, 2009 (received for review June 12, 2009)

Heart tissue possesses complex structural organization on multiple scales, from macro- to nano-, but nanoscale control of cardiac function has not been extensively analyzed. Inspired by ultrastructural analysis of the native tissue, we constructed a scalable, nanotopographically controlled model of myocardium mimicking the in vivo ventricular organization. Guided by nanoscale mechanical cues provided by the underlying hydrogel, the tissue constructs displayed anisotropic action potential propagation and contractility characteristic of the native tissue. Surprisingly, cell geometry, action potential conduction velocity, and the expression of a cell–cell coupling protein were exquisitely sensitive to differences in the substratum nanoscale features of the surrounding extracellular matrix. We propose that controlling cell–material interactions on the nanoscale can stipulate structure and function on the tissue level and yield novel insights into in vivo tissue physiology, while providing materials for tissue repair.

action potential | cardiomyocytes | extracellular matrix | nanotopography | tissue engineering

Living cells and tissues can display high sensitivity to local micro- and nanoscale molecular and topographic patterns, including those provided in vivo by complex and well-defined structures of extracellular matrix (ECM) (1). However, given the small scale of the underlying interactions, their effect on cell and tissue function is far from completely understood. Studies of engineered cell–biomaterial interactions at the subcellular, nanoscale levels are providing evidence for potential importance of submicrometer cues for cell signaling (2), adhesion (3–5), growth (6), and differentiation (7, 8). However, these initial attempts at engineering control of cell function have frequently not been bioinspired or biomimetic and have failed to reproduce the multiscale effects of complex ECM structures (e.g., networks of fibers and components of the basement membrane) and associated chemical ligands, which control integrated multicellular ensembles on scales ranging from a few nanometers to hundreds of micrometers (9, 10). Recent advances in nanofabrication techniques can enable the design and fabrication of scalable scaffolding materials mimicking the structural and mechanical cues present in the in vivo ECM environment (1, 11).

The myocardium is an ensemble of different cell types embedded in the complex and well-defined structures of the ECM and arranged in nanoscale topographical and molecular patterns. Although the structure of cardiac tissue is highly organized in vivo, cardiomyocyte ensembles lose their native organization and adopt random distribution when cultured in vitro by using common culturing techniques, potentially compromising many of their physiological properties. A variety of methods such as mechanical stretching (12), microcontact printing (13), and electrical stimulation (14) have been used to engineer better organized cardiomyocyte cultures. Both 2D and 3D substrata with the ~10 μm feature size have been employed to direct cardiomyocytes into anisotropic arrangements for electrophysiological and mechanical characterization (13, 15–18). However, it is likely that the structure and function of the in vivo cardiac tissue are regulated by much smaller, nanoscale cues provided by the ECM, which might exercise complex, multiscale control of cell and tissue function. Thus, it is important to investigate whether finer control over the cell–material interface on the nanoscale facilitates the creation of truly biomimetic cardiac tissue constructs that recapitulate the structural and functional aspects of the in vivo ventricular myocardial phenotype. In addition, the ability to robustly and reproducibly generate uniformly controlled (both structurally and functionally) and precisely defined engineered cardiac tissue will likely be necessary for eventual therapeutic products.

To address this challenge, here we report the development and analysis of a nanotopographically controlled in vitro model of myocardium that mimics the structural and functional properties of native myocardial tissue and specifically the underlying ECM architecture. The result is an anisotropically nanofabricated substratum (ANFS) formed from scalable, biocompatible polyethylene glycol (PEG) hydrogel arrays, closely imitating the myocardial ECM and allowing formation of engineered cardiac tissue constructs. We investigated the mechanical and electrophysiological function of the engineered cardiac tissue constructs, demonstrating that they faithfully mimic the highly organized function seen in normal heart tissue in vivo. Moreover, strikingly, we found that the engineered tissue structure and function were highly sensitive to variation of the nanoscale topographic features of the substratum, revealing an unexpected level of mechanical regulation.

Results

To explore in detail the myocardial tissue organization, we performed ultrastructural analysis of ex vivo rat myocardium. The results suggest not only that there are identifiable anisotropic arrays of highly elongated and well-aligned cells in the myocardial layer adjacent to an ECM fiber layer (Fig. 1*A* and *B*), but that, strikingly, the cell orientations strongly correlate with the direction of alignment of the matrix fibers immediately underneath (Fig. 1*B* and *C*). This observation suggests that the ECM organization in vivo might provide nanotopographic cues guiding myocardial alignment during cardiovascular development and tissue remodeling and thus exercise precise control over various aspects of tissue organization and function. To test this hypothesis, we constructed an ANFS designed to mimic in 2D the mechanical and topographical features of cardiac matrix fibers and investigated its ability to guide structural and functional cardiac anisotropy.

Author contributions: D.-H.K., K.-Y.S., L.T., and A.L. designed research; D.-H.K., E.A.L., P.K., R.C., S.E., and M.D. performed research; D.-H.K., E.A.L., and R.C. analyzed data; and D.-H.K., E.A.L., K.-Y.S., L.T., and A.L. wrote the paper.

The authors declare no conflict of interest.

This article is a PNAS Direct Submission.

[1]D.-H.K and E.A.L contributed equally to this work.

[2]To whom correspondence may be addressed. E-mail: sky4u@snu.ac.kr, ltung@jhu.edu, or alev@jhu.edu.

This article contains supporting information online at www.pnas.org/cgi/content/full/0906504107/DCSupplemental.

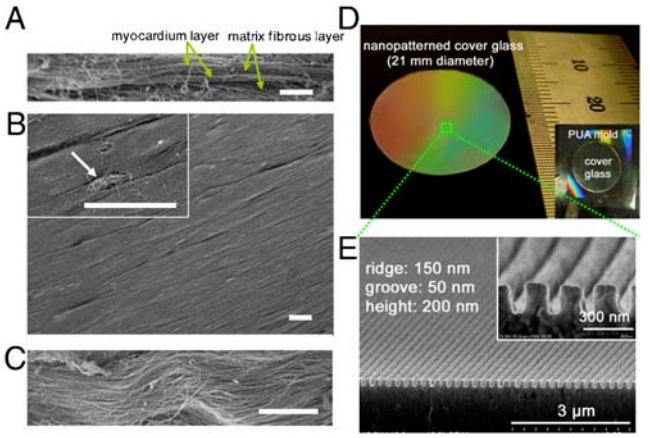

Fig. 1. Rational design and fabrication of nanopatterned substratum of PEG hydrogels. (*A–C*) SEM images of ex vivo myocardium of adult rat heart. Side view (*A*) and top view (*B*) show well-aligned myocardium. The *Inset* in (*B*) and the magnified view in (*C*) demonstrate that the structural organization of the myocardium correlates with matrix fibers aligned in parallel beneath. (*D*) Photograph of a large-area (~3.5 cm^2) ANFS on a glass coverslip. (*E*) Cross-sectional SEM image of the ANFS. [Scale bar: 5 μm in (*A*); 10 μm in (*B*) and (*C*).]

We aimed for the ANFS to be scalable in size, so that the nanoscale definition of features could be extended to tissue dimensions. We thus fabricated square centimeter-sized nanopatterned substrata of PEG-based polymers with precisely defined nanoscale topographic features, extending the nanoscale control over about 5 orders of magnitude in length scale. The PEG hydrogel used for ANFS construction provides a compliant and highly hydrated environment similar to soft tissues having a high water content, thus facilitating diffusion of nutrients and cellular waste through the elastic network (19). We nanofabricated an ANFS of PEG diacrylate (DA) hydrogels by using poly(urethane acrylate) (PUA) molds and a UV-assisted capillary molding technique (20, 21) (Fig. S1*A*; see *SI Methods* for details).

Our ultrastructural analysis of the myocardial ECM (Fig. 1*B* and *C*) suggests that it is composed of aligned fibrils approximately 100 nm in diameter, consistent with previous reports of collagen fibrils varying in diameter in the 30–120-nm range (22). To account for the scale of the ECM cues and possible variability in the diameter of the ECM fibrils, we varied the widths of the grooves and ridges in the designed patterns from 150_50 to 800_800 nm (ridge width_groove width) and from 200 to 500 nm in height (Fig. 1*E*, Fig. S1*B–E*, and Table S1). This range of the variation of the feature sizes allowed us in particular to mimic the likely highly variable distances between individual fibrils and the possibility that several fibrils might be closely apposed and thus perceived by a cell as a feature of the size a few fold larger than 100 nm. The large scale of the designed patterns (~3.5 cm^2) (Fig. 1*D*) allowed us to perform functional analysis (macroscopic contraction and action potential propagation) and biochemical assays of the resulting cardiomyocyte monolayers.

We then cultured neonatal rat ventricular myocytes (NRVMs) on the ANFS for 6–14 days, seeded at a cell density (2.6×10^5 cells/cm^2) leading to near confluence of the cells. We found that, over the first 48 hr after cell seeding, the NRVMs progressively aligned with the ridge and groove features of all the ANFS variants tested to form macroscopic anisotropic arrays, whereas NRVMs on unpatterned substrata maintained a random orientation (Fig. 2*A* and *B* and Movie S1). The confluent NRVM sheets began to contract spontaneously after approximately 2 days of culture and continued to contract throughout the experiment (Movie S2).

Scanning electron micrographs of NRVMs cultured on the ANFS confirmed the formation of cardiomyocyte monolayers interconnected by intercellular junctional structures that were well aligned with the underlying ridge/groove patterns in the ANFS (Fig. 2*C*). To quantify the influence of the ANFS on the assembly

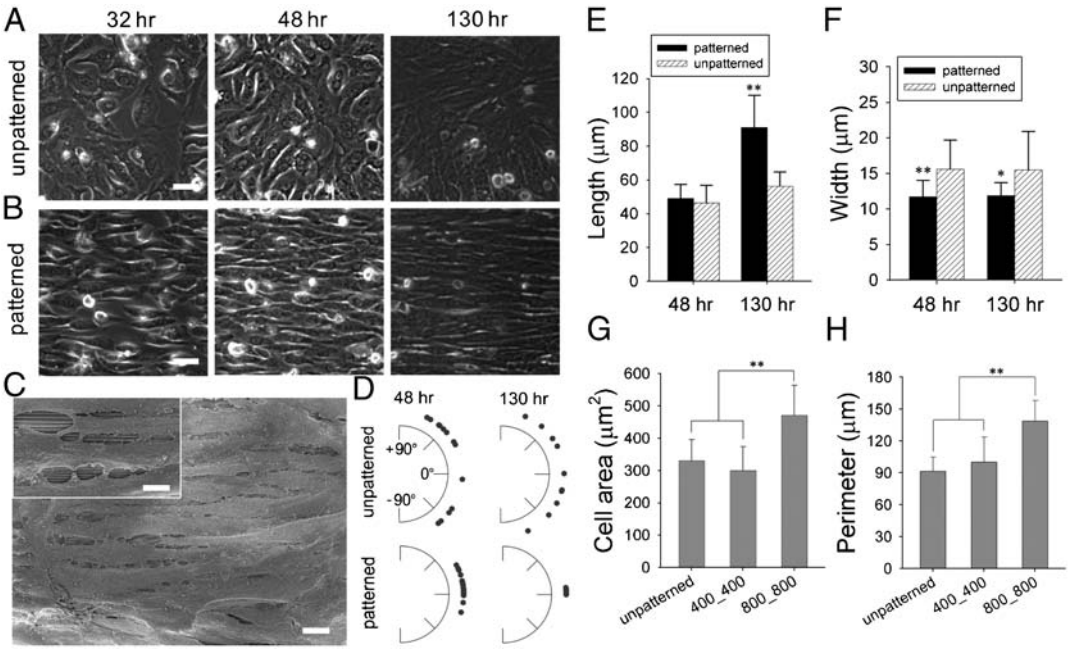

Fig. 2. Formation of confluent monolayers with controlled macroscopic alignment on the ANFS. Phase contrast imaging of NRVMs was performed to show cell growth at 32, 48, and 130 hr on the (*A*) unpatterned substrata and (*B*) ANFS (in this and other figures, the ANFS is 400_400 nm unless otherwise specified). (*C*) SEM image of NRVMs cultured on the ANFS showing anisotropic nanopatterns, aligned cardiomyocytes, and intercellular junctional structures. The *Inset* in (*C*) shows the transverse interconnectivity of the cells. (*D*) Quantification of cell orientation on the ANFS vs. unpatterned substrata. Each dot represents a single cell, and an orientation of 0° represents perfect alignment with the ridge/groove direction. Quantification of the (*E*) myocyte length and (*F*) width on the ANFS vs. the unpatterned substratum. Quantitative comparison of the (*G*) cell projected area and (*H*) perimeter between two different ridge/groove ratios (400_400 vs. 800_800 nm, $n = 33$ for each group). Error bars in (*E–H*) represent the SD about the means. $^{*}p < 0.005$; $^{**}p < 0.0005$. [Scale bar: 5 μm in (*A–C*).]

of the aligned cell monolayer, we measured the orientation, length, and width of cardiac cells in the monolayer over the 5 days after cell seeding. After 2 days NRVMs were generally oriented in the direction of the ridges/grooves, with the coalignment becoming progressively tighter with time (compare Fig. 2*D Lower Left* to *Lower Right*). In contrast, cardiomyocytes on unpatterned substratum exhibited a wide distribution of myocyte orientations at all times.

Myocytes on ANFS (e.g., 400_400 nm groove_ridge widths pattern) were considerably longer than those on the unpatterned substratum. After 5 days, the average myocyte length (91 ± 19 μm, $n = 30$) was about 1.6-fold longer than the average myocyte length on the unpatterned substrata (56 ± 8 μm, $n = 15$) (Fig. 2*E*), and the average width (12 ± 2 μm, $n = 30$) was slightly but significantly narrower ($^{*}p < 0.005$, *t* test) than on unpatterned substrata (15 ± 5 μm, $n = 15$) (Fig. 2*F*), suggesting that ANFS promotes the cell elongation characteristic of organized myocardium. Interestingly, a significant increase in both cell size (Fig. 2*G*) and perimeter (Fig. 2*H*) was observed for 800_800 vs. 400_400 nm patterns ($n = 30$ for each group, $^{**}p < 0.0005$), suggesting that the topographic parameters of the biomaterial surface at the nanoscale may govern cell geometry. Together, these results demonstrate that ANFS can guide self-assembly of cell monolayers into an aligned architecture that mimics the structure of native myocardial tissue. Moreover, the results suggest that the specifics of the nanotopographic pattern can control the average cell size and, thus, the coverage of the available area by cells, thereby potentially controlling cell–cell coupling.

Immunohistochemical analysis showed that actin microfilaments (*F*-actin) and sarcomeric α-actinin in the cells were aligned along the direction of nanoridges/grooves (Fig. 3*A* and Movie S3), in contrast to their random distribution in cells on the unpatterned substrata (Fig. S2*A* and Movie S4). Transmission electron microscopy (TEM) also revealed alignment of myofilaments (Mf) in the direction of the ANFS (Fig. 3*B*), with actin fiber bundles closely following individual ridges (Fig. S2*B*) and grooves (Fig. 3*C*, white arrow) and focal adhesions often forming at the sides of the ridges and grooves (Fig. 3*C*, white arrow head). These results were confirmed by immunohistochemical analysis (Fig. S3), suggesting that anisotropic cell–ECM interaction induced extensive geometrical alteration in focal adhesion assembly and cytoskeletal alignment.

TEM analysis also revealed that, on the 400_400 nm substratum, cells appeared to extend downward toward the groove floor, but this "sagging" was incomplete (Fig. 3*D*). By contrast, the sagging of the cells into the grooves of the 800_800 nm pattern appeared to fill the grooves more completely, with focal adhesions present throughout the cell–groove interface (Fig. 3*E*), suggesting a more extensive cell–ANFS adhesion surface. Because the limited width of the grooves can also limit the length of the actin fibers formed perpendicular to the ANFS orientation, the extent of cell penetration into the grooves can serve to increase the fraction of longer and more functional periplasmic actin fibers running in parallel with the ANFS orientation. Indeed, our TEM analysis revealed that actin fibers running along the grooves were longer and better organized than actin fibers running perpendicular to the grooves in different ANFS patterns (Fig. 3*C*). Together, our findings suggest that nanotopographic control by the ANFS mediates the geometric orientation of focal adhesion assembly, which recruits cytoskeletal molecules into aligned focal adhesion sites. This recruitment likely induces alignment of individual cardiac cells, resulting in the macroscopic alignment of the confluent anisotropic cell monolayer in the model cardiac tissue. The nanoscale width of the grooves can also limit cell penetration into them, thus limiting the cell–substratum adhesion.

Our results suggest that, depending on the size features of the underlying nanotopographic pattern, cardiomyocytes can display different degrees of penetration into the nanogrooves and, as a consequence, differential cell–substratum adhesion. Indeed, the adhesion was sufficiently robust for the cells to not detach from

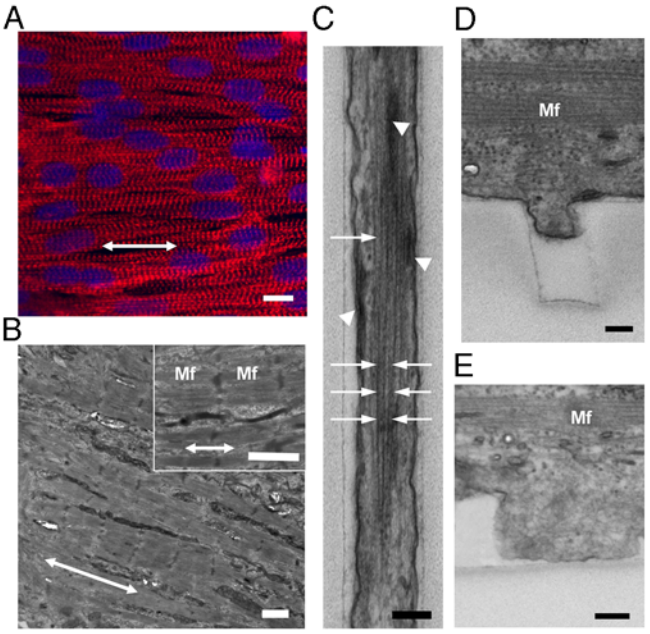

Fig. 3. Cell and cytoskeleton alignment and striations. (*A*) Immunofluorescent images of sarcomeric α-actinin (in red) of NRVMs cultured on the ANFS. Cell nuclei are shown in blue. (*B*) Cross-sectional TEM images of the engineered myocardial tissue grown on the ANFS showing aligned Mf with elongated sarcomeres. Double-headed arrows in (*A*) and (*B*) denote the direction of anisotropic nanopatterns consisting of ridges and grooves. (*C*) An enlarged view of actin bundles (white arrows) and focal adhesions (dark and thick lines indicated by white arrowheads) preferentially formed in parallel to the individual ridges and grooves of the ANFS. (*D–E*) Representative cross-sectional view of the PEG sidewalls showing the lower extent of cell protrusion into (*D*) a 400-nm-wide groove than of that into (*E*) an 800-nm-wide groove. [Scale bar: 10 μm in (*A*); 1 μm in (*B*); 200 nm in (*C–E*).]

the nanotopographically defined substratum over time in culture in all experiments, unlike what has been reported on flat surfaces (23). As cells undergo spontaneous contraction, the resistance to the contracting forces and thus the mechanical stretching experienced by cells likely vary on 400_400 vs. 800_800 nm patterns. Differential mechanical stress and resulting cell stretch can result in varying levels of expression of the major gap junction (GJ) protein connexin 43 (Cx43) (24). We thus experimentally determined if the substratum nanotopography affects the quantity and distribution of Cx43. Consistent with our hypothesis, we found that, with increasing ridge and groove widths, the quantity of Cx43 expression dramatically increased (Fig. 4*A*). Specifically, NRVMs cultured on the 800_800 nm ANFS had the highest level of Cx43 expression (39% adjusted volume on the basis of band intensity measurement) vs. the 400_400 nm ANFS (12%) and the unpatterned substratum (7%). Immunostaining for Cx43 showed that GJs were markedly aligned along the perimeter of the elongated cardiomyocytes cultured on all nanopatterned substrata, resulting in a spatial distribution of Cx43 primarily oriented parallel to the nanoridges (Fig. 4*B*), vs. a more random distribution on unpatterned substrata (Fig. S4*A*). As expected, confocal microscopic 3D images of immunostained Cx43 showed areas of tight intercellular contact punctuated by Cx43 patches indicative of well-formed GJs (Fig. S4*B* and Movie S5), a finding confirmed further by scanning electron microscopy (SEM) analysis (Fig. 2*C*, *Inset*). This finding was also supported by TEM analysis of cell–cell junctions in both the transverse (Fig. S4*C*) and longitudinal directions (Fig. 4*C*) of the nanopattern.

The observed structural changes in organization of cardiomyocyte monolayers on the ANFS suggest that the functional characteristics of the resulting model cardiac tissue, such as its mechanical contraction, can also be strongly affected by the underlying

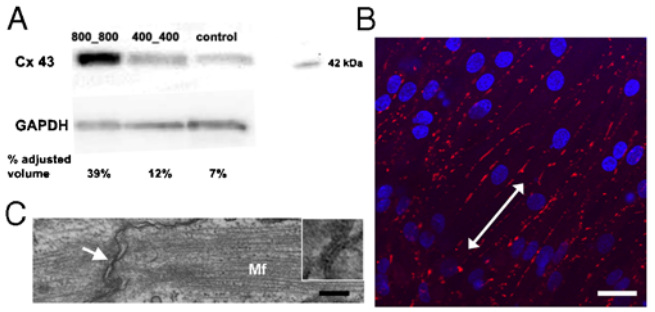

Fig. 4. Spatial regulation of GJ formation. (*A*) Western blot analysis of Cx43 expression on the ANFS with different ridge groove widths. (*B*) Immunofluorescent images of the stained Cx43 of NRVMs on the ANFS. (*C*) TEM image of GJs aligned with the nanopatterns. The *Inset* in (*C*) denotes the GJs at the longitudinal end of two adjacent cells indicated by white arrow. [Scale bar: 20 μm in (*B*); 200 nm in (*C*).]

nanotopography. By tracking the motion of fluorescent beads immobilized on top of contracting NRVM monolayers, we measured the displacement map (Fig. 5*A* and *C*), which was then used to calculate the average direction of the local contraction and its variance as presented in circular plots (Fig. 5*B* and *D*). The results indicate that on unpatterned substrata the direction of contraction varied randomly across the monolayer (Fig. 5*A* and *B* and Movie S6), whereas on the 400 400 nm ANFS the direction of contraction was closely aligned with the longitudinal direction of the ANFS (Fig. 5*C* and *D* and Movie S7), the property also holding on ANFSs of all other dimensions (Fig. S5). These results show that the directional alignment of cardiomyocytes induced by the substratum nanotopography also translates into aligned contractions, which are crucial to the ability of engineered cardiac tissue constructs to generate force (12). Interestingly, although

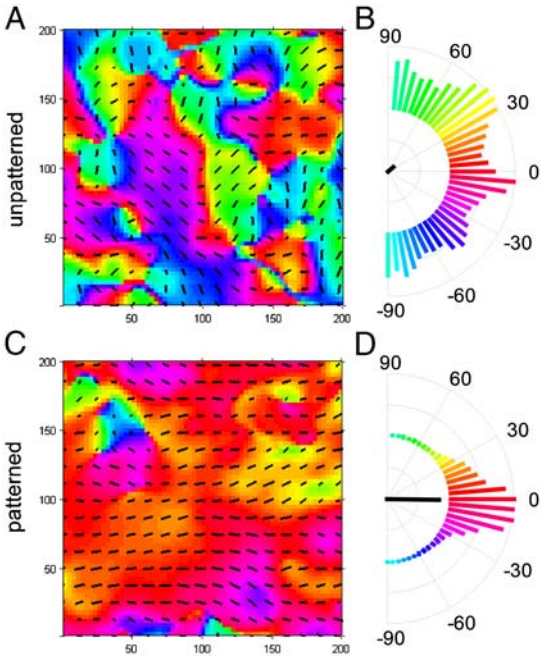

Fig. 5. Contraction analysis of NRVM monolayers cultured on (*A*, *B*) unpatterned substrata and (*C*, *D*) the ANFS. A map of the contraction direction for (*A*) unpatterned substrata and (*C*) the ANFS is shown. The direction of contraction at each spot (*A*, *C*) is indicated by the color [coded to the histograms in (*B*) and (*D*)] as well as by the overlaid vector field. Semicircular histograms of contraction angles (*B*, *D*) indicate the overall directionality of contracting NRVMs on (*B*) the unpatterned substrata and (*D*) the ANFS. The black line in the center of the histogram indicates the average contraction angle, and its length indicates the degree to which the distribution is aligned with the average.

the contraction period was not dependent on the ANFS feature size, the average bead displacement per contraction was significantly higher on the 400 400 vs. 800 800 nm patterns, suggesting higher contraction force and/or lower cellular resistance to contractile forces on ANFSs with smaller feature sizes (Fig. S6). The lower resistance would be consistent with lower cell adhesion on the 400 400 vs. 800 800 nm patterns.

An increased cell–cell coupling on the 400 400 vs. 800 800 nm ANFSs due to an augmented cell coverage of the substratum area (an increased average cell size) and a heightened expression of Cx43 suggested that cells on the 800 800 nm substratum might have an enhanced action potential (AP) conduction velocity. To test this, we measured AP propagation on various ANFSs by using multisite optical mapping of cell transmembrane potentials (25). AP propagation across monolayers on unpatterned substrata expanded uniformly away from the point of stimulation (Fig. 6*A* and Movie S8). In contrast, monolayers cultured on ANFSs showed elliptical, anisotropic propagation (Fig. 6*B* and Movie S9). This difference is further illustrated by expressing the results as isochrone maps (5-ms interval) (Fig. 6*A* and *B*, *Right*). For all the ANFSs assessed, we observed directional differences in conduction velocity, with the conduction velocity in the longitudinal direction (LCV) being higher than in the transverse direction (TCV) at all pacing frequencies (from 2 Hz to the maximum capture rate for each monolayer; Fig. S7). For example, for tissue monolayers formed on 400 400 nm ANFSs, the LCV (26 ± 5 cm/sec) at 3-Hz pacing was more than double the TCV (10 ± 2 cm/sec, $n = 4$, $^{*}p < 0.01$), consistent with values estimated in vivo (26). By contrast, the LCV and TCV for monolayers formed on unpatterned substrata were the same (19 ± 7 and 19 ± 7 cm/sec, respectively, $n = 6$ each) (Fig. 6*C* and *D*). Importantly, consistent with our Cx43 results, there was a clear trend toward higher LCV and TCV as the ridge groove widths of the ANFS were increased (Fig. 6*C* and *D*). In addition, the anisotropy velocity ratio (AR) was significantly higher for monolayers on ANFSs encompassing the entire range of ridge groove widths (minimum AR of 2.2 ± 0.4, $^{*}p < 0.05$ compared with the unpatterned group) than for monolayers on unpatterned substrata ($AR = 1.0 \pm 0.1$) (Fig. 6*E*), endowing the monolayers formed on ANFSs with functional properties closer to those of native myocardium (26). These data indicate that nanotopographic control of PEG hydrogels can be used to direct macroscale anisotropic electrophysiological properties of engineered cardiac tissue constructs.

Discussion

Heart tissues display complex organization on multiple scales. On the scale of cell sheets that comprise the myocardium, the directions of myocytes and myofibrils are preferentially aligned, providing a natural direction for exertion of contractile forces and an axis for the fast propagation of APs. In previous studies, mutual cell alignment in 2D cell cultures was primarily achieved on the basis of ad hoc applications of various patterning techniques with microrather than nanofeatures (13, 15–18), not explicitly mimicking the organizing principles of the native heart tissue. In addition, the mechanical properties and the degree of biocompatibility of the materials commonly used as the cell substrata have limited both the therapeutic potential of the designed tissues and their use for a fundamental understanding of the principles of cardiac tissue self-organization. To address these drawbacks, we employed a bioinspired design of a model cardiac tissue, more rationally based on ultrastructural analysis of the native cardiac tissue.

We designed a unique cell substratum on the basis of our observation that the ECM immediately underlying the aligned cell arrays in the native myocardium is present in the form of aligned fibers parallel to the direction of cell alignment. We thus fabricated biocompatible, PEG-based substrata with precisely controlled nanoscale topography, whose overall dimensions extended from

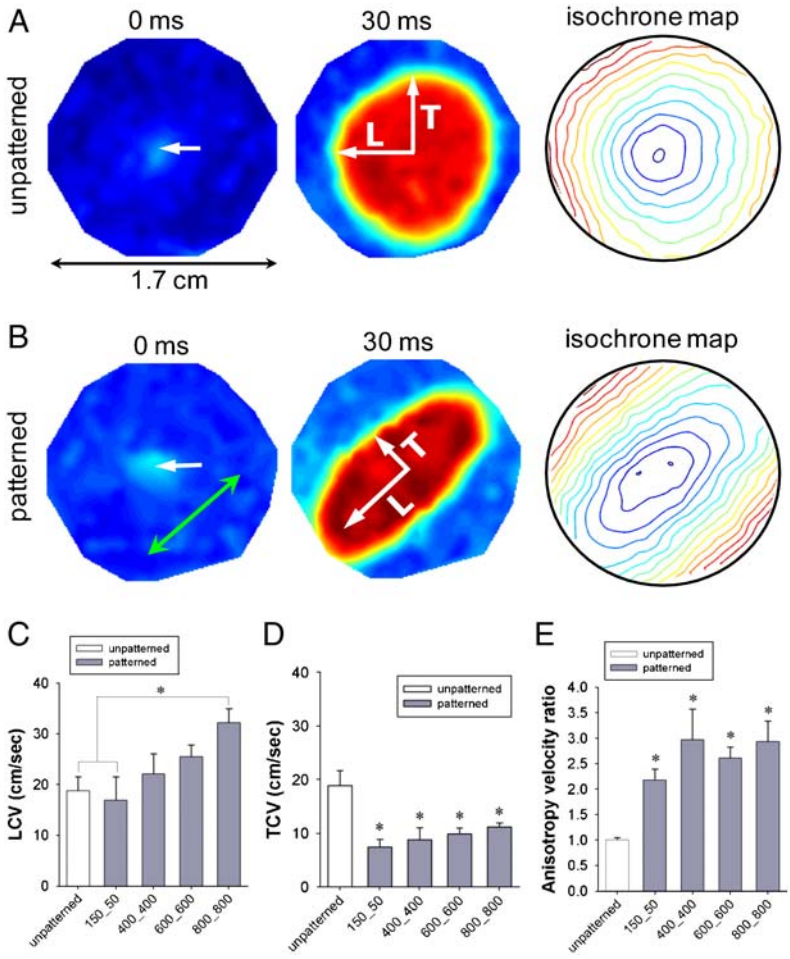

Fig. 6. Electrophysiological characteristics of engineered cardiac tissue construct. AP propagation across monolayers cultured on (*A*) unpatterned substrata and (*B*) the ANFS. Optical maps are 17 mm in diameter. Point stimulation (3 Hz) was applied in the center of the NRVM monolayer at 0 ms (indicated by white arrows). The green arrow indicates the direction of NRVM alignment on the ANFS. Isochrone maps spaced at 5-ms intervals. Increasing the ridge groove width showed a trend toward increasing the (*C*) LCV and (*D*) TCV ($n = 6$ for the unpatterned group, $n = 4$ for each patterned group, $^{*}p < 0.05$ compared with the unpatterned group). In addition, for NRVM monolayers on the ANFS, the LCV was significantly faster than the TCV ($n = 4$ per group, $^{*}p < 0.05$ between the LCV and TCV for 400 400 nm and above). In contrast, NRVM monolayers on unpatterned substrata showed no directional differences in the CV (LCV $= 19 \pm 7$ cm/sec, TCV $= 19 \pm 7$ cm/sec, $n = 6$). (*E*) The ratio of longitudinal to transverse conduction velocity (LCV/TCV) was more than doubled for NRVM monolayers seeded onto patterned substrata (ridge-to-groove ratios ranging from 150 50 to 800 800 nm), as compared with the ratio for unpatterned control substrata ($n = 4$ for patterned groups and $n = 6$ for the unpatterned control group, $^{*}p < 0.05$ compared with the unpatterned group). Error bars in (*C*–*E*) represent the SEM.

the nanometer to centimeter scale, allowing both electrophysiological analysis and biochemical tests (e.g., the immunoblotting assays). We note that compared with other nanolithographic methods, such as electron beam lithography (27), x-ray lithography (28), and scanning probe lithography (29), the advantages of the capillary lithography-based approach used here are in its increased reproducibility, scalability, and cost effectiveness.

These substrata indeed caused NRVMs to form highly anisotropic cell arrays guided by the direction of the underlying nanoridges. This finding suggests that, although a single cell's width allows it to span 10 or more nanoridges, the cell is still guided by the directionality of this topographic cue. The underlying mechanism of this effect is likely similar to the shape control of other cell types on nanotopographically defined substrata (6, 30), owing to a strong influence of the nanoridges and nanogrooves on the organization of focal adhesions and cortical cytoskeleton, as confirmed by our analysis.

Given that the feature sizes of the nanopatterned substratum were much smaller than those used in previous studies and that individual cells can span multiple nanoridges, a surprising finding was that various cell and model tissue properties were sensitive to the exact nature of the nanotopographic pattern. In particular, we found considerable differences in features implicated in cardiac tissue function, including cell geometry, conduction velocity, and expression of Cx43 (Table S2). These findings are especially intriguing, because they suggest that the cardiac cell and tissue structure and function may be sensitive to the exact nanoscale organization and composition of the ECM. The differential responses to the nanotopographic patterns likely stem from the differing degree of penetration of the cells into the nanogrooves (Fig. 3*D* and *E*), as suggested to explain the differential gecko-inspired nanopattern–cell interactions described previously (31). This difference in the cell–substratum interface might place distinct spatial constraints on cellular organization (due to the spatial confinement of a groove), e.g., on the direction and degree of actin polymerization and focal adhesion formation. Furthermore, because cells cultured on the 400 400 nm pattern do not entirely envelop the groove surface, they have more limited exposure to the ECM vs. larger patterns, limiting their adhesion and spreading. The relative increase of cell spreading on the 800 800 nm surfaces can have two important consequences: (*i*) Because they spread more (have higher area), the number of intercellular gaps (open spaces) would be smaller vs. the 400 400 nm ANFS, if the same numbers of cells are seeded on both surfaces; therefore the intercellular distance will increase, which can lead to enhancement of cell–cell coupling. (*ii*) The cells on the 800 800 nm ANFS can experience different stretching due to their own active contractility, which, as in cases of exogenously applied stress (24), might rapidly and strongly augment Cx43 expression, as indeed observed in our analysis; this will lead to an even better cell–cell coupling and a decreased resistance to AP propagation and, thus, higher velocities of AP propagation. This possibility agrees well with our experimental observations and furthermore suggests that there is an optimal topography for cell–cell coupling, which maximizes the area of cell–substratum contact. If the grooves are too narrow, the contact is low due to limited cell penetration into the groove; if the grooves are too wide, or the substratum is flat, cells can lose the extra contact area provided by the 3D topography (see Fig. 7 for a summary of this mechanism). We also note that this mechanism emphasizes the importance of the degree of separation between individual ridges that mimics the variable local separation between individual ECM fibrils.

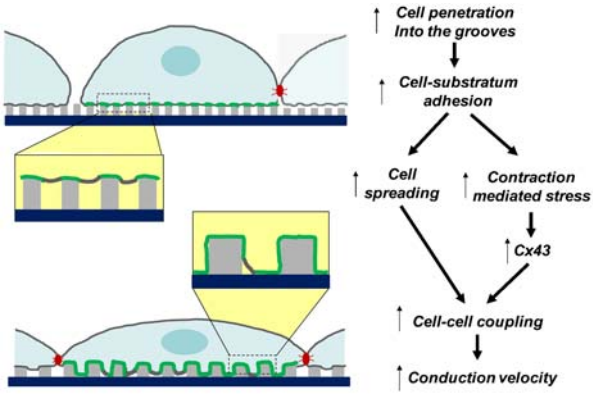

Fig. 7. Model of the sensitivity of structural and functional properties of the cardiac constructs to the details of the underlying nanostructured substrata. Areas of direct plasma membrane–substratum contact are highlighted in green, and gap junctional complexes are shown in red. Areas of the cell–substratum interfaces are magnified for clarity.

It might be of interest to contrast the response of model cardiac tissues on micro- vs. nanopatterned cell substrata. On microscale patterns used thus far, the width of a single myocyte is typically less than or equal to the width of the parallel pattern bands that are permissive for cell attachment. Furthermore, the width of the gaps between the permissive pattern bands is also typically equal to or larger than the cell width, which can severely limit cell–cell coupling in the direction transverse with respect to the pattern orientation. This arrangement contrasts with the uninhibited cell–cell contact in the TCV observed in our experiments. It is perhaps for this reason that, in experiments using microabrasion to form a patterned substratum, an increase in the LCV with groove width and depth was accompanied by no change or a slight decrease in the TCV (13), whereas on the ANFS both the LCV and TCV increased by the same extent with the feature size.

Our results strongly suggest that, to recapitulate more natural conditions controlling the structural and functional properties of cardiac tissue constructs, one may need to operate on a scale much smaller than the tens to hundreds of micrometer feature sizes commonly used so far, i.e., on the nanoscale characteristic of the ECM structure. Analysis on this scale would also be consistent with the increasing evidence of exquisite sensitivity of living cells to size-dependent nanoscale stimulation (8, 32, 33). The high degree of sensitivity of the cell and tissue structure to the nanoscale substratum topography can present a powerful control mechanism for engineering the desired functionality of model anisotropic cardiac tissues, allowing, for example, local changes in the conduction properties with nanoscale precision. The biocompatibility of the material used to fabricate tissue substrata and the scalability of the resulting patterns with scales spanning 5 orders of magnitude (from 10^{-7} m feature size to 10^{-2} m substratum size) open up the opportunities to directly use it as a scaffold for construction of implantable engineered cardiac tissue. This scaffold might include using the monolayered constructs described here or extending the engineering to three-dimensional devices following the recently proposed methodology (34).

Materials and Methods

Nanopatterned substrata of PEG hydrogels were fabricated by using UV-assisted capillary lithography-based nanomolding techniques as previously described (20). NRVMs were isolated as previously described (13) and then cultured on the nanopatterned PEG substratum to form the confluent monolayer. Optical mapping, contraction mapping, Western blot, SEM/TEM analysis, and immunostaining experiments were performed 6–7 days after plating. Quantitative analysis of conduction velocity and contraction was performed by using custom-written MATLAB scripts. Details are described in the *SI Text*.

ACKNOWLEDGMENTS. The authors thank B. Eaton, W. Limpitkul, and R. Smith for their technical assistance. This work was supported by National Institutes of Health Grants 1R21EB008562-01A1 (to A.L.) and R01HL66239 (to L.T.) and the World Class University program (R31-2008-000-10083-0) and the Center for Nanoscale Mechatronics and Manufacturing (08K1401-00210) funded by the Ministry of Education, Science and Technology of Korea (K.Y.S.). D.-H.K. was supported by American Heart Association Predoctoral Fellowship 0815104E. E.A.L. was supported by NIH training Grant T32-HL07581.

1. Stevens M, George J (2005) Exploring and engineering the cell surface interface. *Science*, 310:1135–1138.
2. Mannix RJ, et al. (2008) Nanomagnetic actuation of receptor-mediated signal transduction. *Nat Nanotechnol*, 3:36–40.
3. Karuri NW, et al. (2004) Biological length scale topography enhances cell-substratum adhesion of human corneal epithelial cells. *J Cell Sci*, 117:3153–3164.
4. Cavalcanti-Adam EA, et al. (2007) Cell spreading and focal adhesion dynamics are regulated by spacing of integrin ligands. *Biophys J*, 92:2964–2974.
5. Koo LY, Irvine DJ, Mayes AM, Lauffenburger DA, Griffith LG (2002) Co-regulation of cell adhesion by nanoscale RGD organization and mechanical stimulus. *J Cell Sci*, 115:1423–1433.
6. Yim EK, et al. (2005) Nanopattern-induced changes in morphology and motility of smooth muscle cells. *Biomaterials*, 26:5405–5413.
7. Dalby MJ, et al. (2007) The control of human mesenchymal cell differentiation using nanoscale symmetry and disorder. *Nat Mater*, 6:997–1003.
8. Park J, Bauer S, von der Mark K, Schmuki P (2007) Nanosize and vitality: TiO_2 nanotube diameter directs cell fate. *Nano Lett*, 7:1686–1691.
9. Geiger B, Bershadsky A, Pankov R, Yamada KM (2001) Transmembrane crosstalk between the extracellular matrix—Cytoskeleton crosstalk. *Nat Rev Mol Cell Biol*, 2:793–805.
10. Abrams GA, Murphy CJ, Wang ZY, Nealey PF, Bjorling DE (2003) Ultrastructural basement membrane topography of the bladder epithelium. *Urol Res*, 31:341–346.
11. Park H, et al. (2007) Nanofabrication and microfabrication of functional materials for tissue engineering. *Tissue Eng*, 13:1867–1877.
12. Fink C, et al. (2000) Chronic stretch of engineered heart tissue induces hypertrophy and functional improvement. *FASEB J*, 14:669–679.
13. Bursac N, Parker KK, Iravanian S, Tung L (2002) Cardiomyocyte cultures with controlled macroscopic anisotropy: A model for functional electrophysiological studies of cardiac muscle. *Circ Res*, 91:e45–54.
14. Radisic M, et al. (2004) Functional assembly of engineered myocardium by electrical stimulation of cardiac myocytes cultured on scaffolds. *Proc Natl Acad Sci USA*, 101:18129–18134.
15. Fast VG, Darrow BJ, Saffitz JE, Kleber AG (1996) Anisotropic activation spread in heart cell monolayers assessed by high-resolution optical mapping. Role of tissue discontinuities. *Circ Res*, 79:115–127.
16. Bien H, Yin L, Entcheva E (2003) Cardiac cell networks on elastic microgrooved scaffolds. *IEEE Eng Med Biol Mag*, 22:108–112.
17. McDevitt TC, et al. (2002) In vitro generation of differentiated cardiac myofibers on micropatterned laminin surfaces. *J Biomed Mater Res*, 60:472–479.
18. Gopalan SM, et al. (2003) Anisotropic stretch-induced hypertrophy in neonatal ventricular myocytes micropatterned on deformable elastomers. *Biotechnol Bioeng*, 81:578–587.
19. Watkins AW, Anseth KS (2005) Investigation of molecular transport and distributions in poly(ethylene glycol) hydrogels with confocal laser scanning microscopy. *Macromolecules*, 38:1326–1334.
20. Kim P, et al. (2005) Fabrication of nanostructures of polyethylene glycol for applications to protein adsorption and cell adhesion. *Nanotechnology*, 16:2420–2426.
21. Kim DH, et al. (2009) Guided cell migration on microtextured substrates with variable local density and anisotropy. *Adv Funct Mater*, 19:1579–1586.
22. Perumal S, Antipova O, Orgel JP (2008) Collagen fibril architecture, domain organization, and triple-helical conformation govern its proteolysis. *Proc Natl Acad Sci USA*, 105:2824–2829.
23. Khademhosseini. A, et al. (2007) Microfluidic patterning for fabrication of contractile cardiac organoids. *Biomed Microdevices*, 9:149–157.
24. Teunissen BE, Jongsma HJ, Bierhuizen MF (2004) Regulation of myocardial connexins during hypertrophic remodelling. *Eur Heart J*, 25:1979–1989.
25. Lim ZY, Maskara B, Aguel F, Emokpae R, Jr, Tung L (2006) Spiral wave attachment to millimeter-sized obstacles. *Circulation*, 114:2113–2121.
26. Bursac N, et al. (1999) Cardiac muscle tissue engineering: Toward an in vitro model for electrophysiological studies. *Am J Physiol*, 277:H433–444.
27. Gibson JM (1997) Reading and writing with electron beams. *Physics Today*, 50:56–61.
28. Silverman JP (1998) Challenges and progress in x-ray lithography. *J Vac Sci Technol B*, 16:3137–3141.
29. Salaita K, Wang YH, Mirkin CA (2007) Applications of dip-pen nanolithography. *Nat Nanotechnol*, 2:145–155.
30. Teixeira AI, Abrams GA, Bertics PJ, Murphy CJ, Nealey PF (2003) Epithelial contact guidance on well-defined micro- and nanostructured substrates. *J Cell Sci*, 116:1881–1892.
31. Mahdavi A, et al. (2008) A biodegradable and biocompatible gecko-inspired tissue adhesive. *Proc Natl Acad Sci USA*, 105:2307–2312.
32. Jiang W, Kim BY, Rutka JT, Chan WC (2008) Nanoparticle-mediated cellular response is size-dependent. *Nat Nanotechnol*, 3:145–150.
33. Oh S, et al. (2009) Stem cell fate dictated solely by altered nanotube dimension. *Proc Natl Acad Sci USA*, 106:2130–2135.
34. Ohashi K, et al. (2007) Engineering functional two- and three-dimensional liver systems in vivo using hepatic tissue sheets. *Nat Med*, 13:880–885.